Molecules **2013**, *18*, 12687-12706; doi:10.3390/molecules181012687

OPEN ACCESS

molecules

ISSN 1420-3049

www.mdpi.com/journal/molecules

Article

Orbital Interaction and Electron Density Transfer in $Pd^{II}([9]aneB_2A)L_2$ Complexes: Theoretical Approaches

Ock Keum Kwak [1], Mahreen Arooj [1], Yong-Jin Yoon [2], Euh Duck Jeong [3] and Jong Keun Park [1,*]

[1] Department of Chemistry Education and Research Institute of Natural Science, Educational Research Institute Teachers College, Gyeongsang National University, Jinju 660-701, Korea

[2] Department of Chemistry and Research Institute of Natural Science, Gyeongsang National University, Jinju 660-701, Korea

[3] Division of High-Technology Materials Research, Korea Basic Science Institute, Busan 618-230, Korea

* Author to whom correspondence should be addressed; E-Mail: mc7@gnu.ac.kr; Tel.: +82-55-772-2225.

Received: 29 July 2013; in revised form: 13 September 2013 / Accepted: 29 September 2013 / Published: 14 October 2013

Abstract: The geometric structures of Pd-complexes {Pd([9]ane**B**$_2$**A**)**L**$_2$ and Pd([9]ane**BAB**)**L**$_2$ where **A** = P, S; **B** = N; **L** = PH_3, $P(CH_3)_3$, Cl^-}, their selective orbital interaction towards equatorial or axial (soft **A**…Pd) coordination of macrocyclic [9]ane**B**$_2$**A** tridentate to Pd**L**$_2$, and electron density transfer from the electron-rich *trans* **L**-ligand to the low-lying unfilled a_{1g}(5s)-orbital of Pd**L**$_2$ were investigated using B3P86/lanl2DZ for Pd and 6-311+G** for other atoms. The pentacoordinate *endo*-[Pd([9]ane**B**$_2$**A**)(**L**-donor)$_2$]$^{2+}$ complex with an axial (soft **A**--Pd) quasi-bond was optimized for stability. The fifth (soft **A**--Pd) quasi-bond between the σ-donor of soft **A** and the partially unfilled a_{1g}(5s)-orbital of Pd**L**$_2$ was formed. The pentacoordinate *endo*-Pd([9]ane**B**$_2$**A**)(**L**-donor)$_2$]$^{2+}$ complex has been found to be more stable than the corresponding tetracoordinate *endo*-Pd complexes. Except for the *endo*-Pd pentacoordinates, the tetracoordinate Pd([9]ane**BAB**)**L**$_2$ complex with one equatorial (soft **A**-Pd) bond is found to be more stable than the Pd([9]ane**B**$_2$**A**)**L**$_2$ isomer without the equatorial (**A**-Pd) bond. In particular, the geometric configuration of *endo*-[Pd([9]ane**PNP**)(**L**-donor)$_2$]$^{2+}$ could not be optimized.

Keywords: macrocyclic tridentate; position selectivity; steric and electronic effects; orbital interaction; geometric configuration

1. Introduction

Carbon-carbon/carbon-heteroatom (e.g., C–C, C–N, C–O, C–S) bond formation using palladium-mediated cross-coupling reactions has been extensively studied during the last few decades [1–36]. In this context, the achievements in development of novel and efficient synthetic methodologies for these types of reactions have been acknowledged with the 2010 Nobel Prize in Chemistry. Much attention has been paid to the design and development of powerful Pd-catalysts/precursors [1–17,37–43] that contain bulky and electron-rich ligands (such as phosphines and *N*-heterocyclic carbenes, NHCs) and to their potential synthetic applications [18–36] in the Pd-catalyzed cross-couplings of various substrates (such as allyl, aryl, and vinyl halides and olefins). Catalytic activity enhancement of $Pd^{(0)}(\mathbf{L})_n$-precursors is greatly influenced by the electronic and steric properties of electron-rich and bulky **L**-ligands [1–8,18–42]. Due to the electronic effect of the *trans* **L**-donor, the oxidation state of Pd in neutral and anionic $Pd^{(0)}\mathbf{L}_nX$ catalysts is zero. The geometric structure of bulky **L**-ligand affects the oxidative addition reaction of Ar-X to the $Pd^{(0)}(\mathbf{L})_n$-precursor [6–8,25–32].

The geometric structures of the active $RPd(\mathbf{L})_nX$ intermediates produced in various steps of Pd-mediated cross-coupling reactions (e.g., oxidative addition, transmetalation, reductive elimination) have been investigated both theoretically [9–17] and experimentally [18–42]. The oxidative addition of substrates (R-X) to $Pd\mathbf{L}_n$-precursor resulted in penta-, hexa-, and octacoordinate geometries [33–36] of the $RPd^{II}(\mathbf{L})_nX$ intermediates with relative stability and a life time of 30 s [3]. The binding atoms in the penta-, hexa-, and octacoordinate Pd intermediates are not located on the x, y, and z-axis of trigonal bipyramidal, octahedral, and cubic structures. In particular, the geometric conformation of $RPd(\mathbf{L})_nX$ intermediates is altered by the *cis-trans* isomerization of **L**-ligand. The isomerization has been exclusively explained by the energy relationship between the isomers and low potential barrier (or binding energy of Pd-**L**) [3–8,44,45]. However, Goossen *et al*. [14,15] provided no evidence for mechanistic steps involving stable pentacoordinate Pd^{II} intermediates in Pd-mediated cross-coupling reactions. To the best of our knowledge, the relative stabilities of various $RPd(\mathbf{L})_nX$ intermediates produced by oxidative addition of the substrate (R-X) to $Pd\mathbf{L}_n$ and the geometric changes in intramolecular interaction of $RPd^{II}(\mathbf{L})_nX$ have not been investigated.

In previous studies using hemilabile multidentate ligands [37–47], exceptional oxidation state and specific coordination selectivity have been observed for the Pd([9]ane$\mathbf{B}_2\mathbf{A}$)$\mathbf{L}_2$ complexes with mixed soft **A** and hard **B** tridentates. The uncommon geometric structures of Pd([9]ane$\mathbf{B}_2\mathbf{A}$)$\mathbf{L}_2$ complexes with an axial (**A**…Pd) interaction were mainly formed under the following restrictive conditions: (1) coordination bonds of **P**- and **N**-functionalized derivatives are present [18–39] and (2) polymeric side chain interactions exist [40–42]. In the Pd complex with an apical (hard **N**…Pd) interaction [42], the apical interaction was explained by an antibonding interaction between the lone pair of the apical **N** site and the d_{z2}-orbital of the Pd^{II} species. In the ligand exchange reaction of square-planar Pd complexes, a vertical **L**…Pd interaction also has been optimized [43–47]. The mechanism of hydration

exchange processes in the five-coordinate Pd^{II} intermediates suggested two models for the axial interaction: σ-donor…d_z^2-orbital and HOH…d_z^2-orbital. The apical (**A**…Pd) orbital interaction of Pd([9]ane$\mathbf{B_2A}$)$\mathbf{L_2}$ complex in mixed **A** and **B** sites has not been explained very well.

Origins of the unusual coordination structures for the Pd complexes and the configurational changes in the $ArPdL_nX$ intermediates of Pd-mediated cross-coupling reaction have not been explored yet. To investigate these properties, the present study proposed the following geometric structures and the relative stabilities of macrocyclic Pd([9]ane$\mathbf{B_2A}$)$\mathbf{L_2}$ complexes within the frameworks of its orbital interaction and electronic effect. For the Pd-mediated cross-coupling reactions, we suggest a two-step mechanism for the electron density transfer: the abundant electron density of the *trans* **L**-donor may transfer to a low-lying unoccupied $a_{1g}(5s)$-orbital of Pd^{II} and then the partially unfilled $a_{1g}(5s)$-orbital can interact with the Lewis base substrate (σ-donor) as shown in Scheme 1.

Scheme 1. Two-step mechanism for the electron density transfer from an equatorial *trans* **L**-donor {PH_3, $P(CH_3)_3$} and a σ-donor of substrate to a low-lying unoccupied $a_{1g}(5s)$-orbital of the Pd^{II} center.

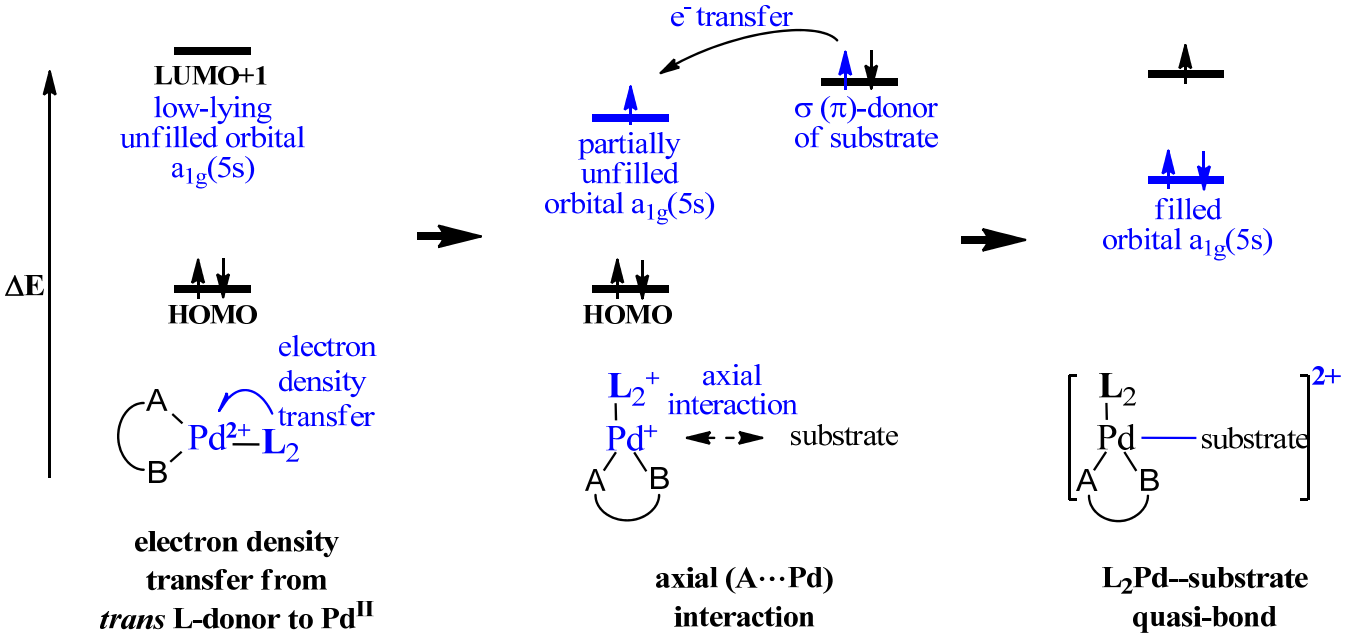

To justify the intermediate step for the additional reaction of [9]ane$\mathbf{B_2A}$ to Pd$\mathbf{L_2}$, the relative stabilities ($\Delta_{exo\text{-}endo}$, $\Delta_{BAB\text{-}B2A}$) and the apical and equatorial orbital interactions [σ-donor…$a_{1g}(5s)$, σ-donor…$4d_{x2\text{-}y2}$] shown in Scheme 2 are suggested in this research exertion. The relative affinity of Pd towards the soft **A** (or hard **B**) in Pd$\mathbf{L_2}$, the electronic characteristics owing to the ***donating*** (or ***withdrawing***) property of the *trans* **L**-ligand, the axial σ-donor…$a_{1g}(5s)$ interaction between the σ-donor of the **A** site and the low-lying unfilled $a_{1g}(5s)$-orbital of $Pd^{II}L_2$, and the relative stability of the uncommon Pd complexes were examined in detail.

Scheme 2. A plausible orbital interaction of an equatorial or axial coordination bond of [9]ane**B**$_2$**A** (or [9]ane**BAB**) with Pd**L**$_2$. (**a**): *exo*-type with an apical site pointing to outside. (**b**): *endo*-type with an apical site pointing to the Pd center. (**c**): *endo*-Pd complex with an apical (**A**…Pd) attraction. (**d**): *endo*-Pd complex without any axial interaction. (**e**): *endo*-Pd complex with an apical (**A**…Pd) repulsion.

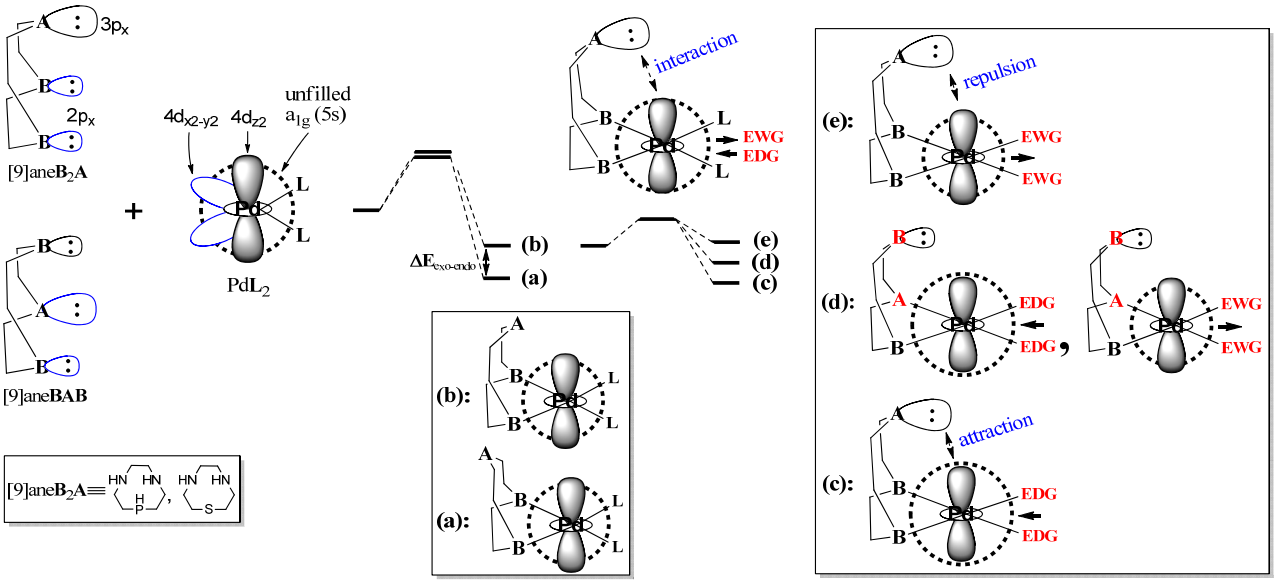

2. Computational Methods

To explore the geometric structure and the relative stability of the Pd complexes, we selected the Pd([9]ane**B**$_2$**A**)**L**$_2$ [**A** = P, S; **B** = N; **L** = donor {PH_3, $P(CH_3)_3$}, acceptor (Cl^-)] complex as a model with [9]ane**B**$_2$**A**, PH_3, $P(CH_3)_3$, and Cl^- groups as ligands. The equilibrium structure of tetracoordinate Pd complexes was fully optimized with the B3P86/6-311+G** (lanl2DZ for Pd) level using Gaussian 03 [48]. The macrocyclic [9]ane**N**$_2$**P** and [9]ane**N**$_2$**S** ligands are 1,4-diaza-7-phospacyclononane and 1,4-diaza-7-thiacyclononane, respectively (as shown in Scheme 2). The hybrid B3P86 density functional utilizes the exchange function of Becke [49,50] in conjunction with the Perdew 1986 correlation function [51] and yields good structural and energetic information, even for relatively large chemical systems such as transition metal complexes. For the optimized equilibrium Pd^{II} complexes, the atomic charges obtained by the CHelpG method were analyzed using atomic radii (H = 0.53 Å, C = 0.67 Å, N = 0.56 Å, O = 0.48 Å, P = 0.98 Å, S = 0.88 Å, Cl^- = 1.67 Å, Pd^{II} = 0.78 Å) [52]. The relative energies of the Pd^{II} complexes were compared. To confirm the existence of stable structures, the harmonic vibration frequencies of the species were analyzed at the B3P86 level. In addition, the geometric structures of *endo*-Pd([9]ane**A**$_2$**B**)**L**$_2$ {**A** = P, S; **B** = N; **L** = PH_3, $P(CH_3)_3$, Cl^-} were optimized at the B3P86/6-311+G** (lanl2DZ for Pd) level. The optimized structures including HOMO and the geometric parameters are described in Supplementary Information Figure S1 and Table S1, respectively. To check the rationality of our results at the effective core potential level for Pd, the geometric structures of the equilibrium Pd complexes were also optimized at the CAM-B3LYP// 6-311+G** (lanl2DZ for Pd) and B3P86/6-311+G** (3-21g* for Pd) levels using Gaussian 09. Further, optimized structures and parameters are given in Supplementary Information Figures S2 and S3 and Tables S2 and S3.

3. Results and Discussion

Optimized geometric structures of Pd([9]ane$\mathbf{B_2A}$)$\mathbf{L_2}$ and Pd([9]ane**BAB**)$\mathbf{L_2}$ types are represented in Figure 1, and their parameters are listed in Table 1. The values of optimized parameters in this study were compared to the values reported previously [17,18,23,37,40–42,44,53,54]. In the Pd complexes, the tetracoordinate structures of both the *endo*- and *exo*-types of structures were optimized. Pd^{II} locates at the center of the tetracoordinate mean plane that is coordinated with a [9]ane$\mathbf{B_2A}$ (or [9]ane**BAB**) tridentate and two monodentate ligands. In the case of the *endo*-[Pd([9]ane$\mathbf{B_2A}$)(**L**-donor)$_2$]$^{2+}$ with *trans* **L**-donor, *endo*-[Pd([9]ane$\mathbf{B_2A}$)(**L**-donor)$_2$]$^{2+}$ pentacoordinates with an axial (**A**--Pd) quasi-bond were stably optimized, and the Pd^{II} center lies slightly above the mean plane. The (**A**--Pd) quasi-bond lengths ($R_{Pd...A}$ = 2.782 ~ 2.935 Å) between the axial **A** site and Pd^{II} center are much shorter than the corresponding bonds in the other *endo*- and *exo*-Pd tetracoordinates. The optimized structure of *endo*-Pd([9]ane$\mathbf{B_2A}$)Cl_2 complex with a *trans* Cl-acceptor has a tetracoordinate geometry. The distances between the axial **A** site and Pd^{II} center are long ($R_{Pd...A}$ = 3.033~3.190 Å). Our values are in agreement with the geometric structures and the apical (soft **A**…Pd) distances ($R_{(Pd...A)}$ = 3.087~3.293 Å) seen in the previous crystal studies [37,40–42].

Figure 1. The geometric structures of the Pd complexes [Pd([9]ane$\mathbf{B_2A}$)$\mathbf{L_2}$ and Pd([9]ane**BAB**)$\mathbf{L_2}$ (**A** = P, S; **B** = N; **L** = PH_3, $P(CH_3)_3$, Cl^-] were optimized at the B3P86/6-311+G** (lanl2DZ for Pd) level. All structures are viewed from the side.

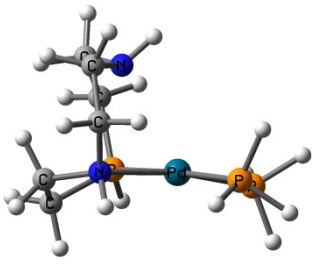

endo-[Pd([9]aneNPN)$(PH_3)_2$]$^{2+}$

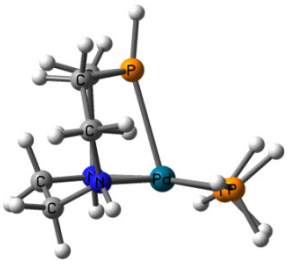

endo-[Pd([9]aneN_2P)$(PH_3)_2$]$^{2+}$

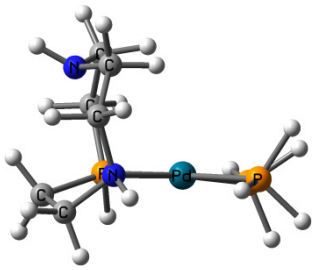

exo-[Pd([9]aneNPN)$(PH_3)_2$]$^{2+}$

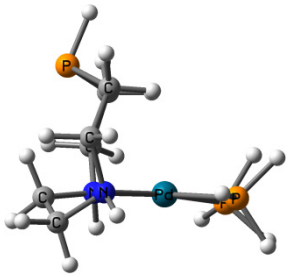

exo-[Pd([9]aneN_2P)$(PH_3)_2$]$^{2+}$

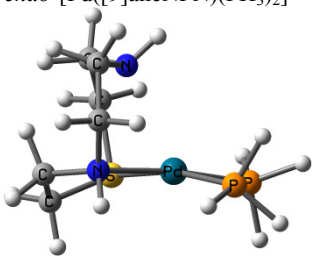

endo-[Pd([9]aneNSN)(PH3)2]$^{2+}$

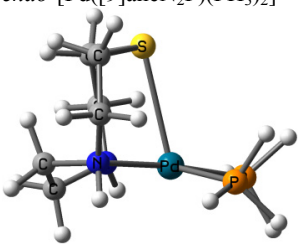

endo-[Pd([9]aneN2S)(PH3)2]$^{2+}$

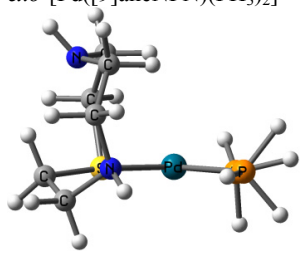

exo-[Pd([9]aneNSN)(PH3)2]$^{2+}$

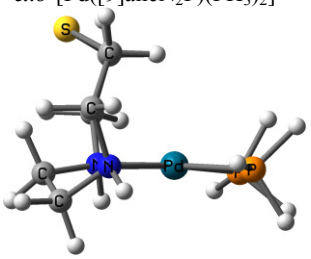

exo-[Pd([9]aneN2S)(PH3)2]$^{2+}$

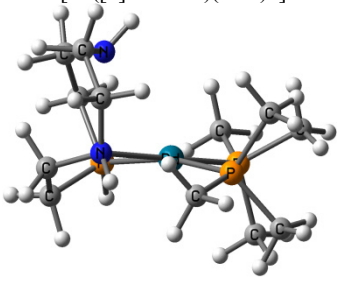

endo-[Pd([9]aneNPN)$\{P(CH_3)_3\}_2$]$^{2+}$

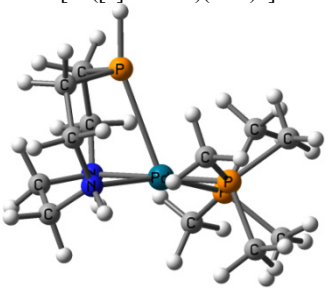

endo-[Pd([9]aneN_2P)$\{P(CH_3)_3\}_2$]$^{2+}$

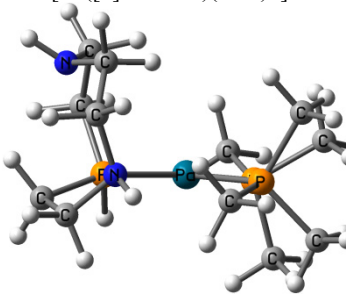

exo-[Pd([9]aneNPN)$\{P(CH_3)_3\}_2$]$^{2+}$

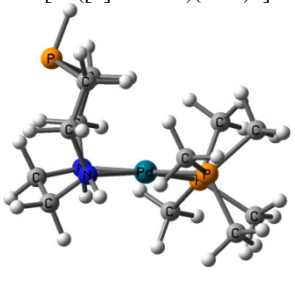

exo-[Pd([9]aneN_2P)$\{P(CH_3)_3\}_2$]$^{2+}$

Figure 1. *Cont.*

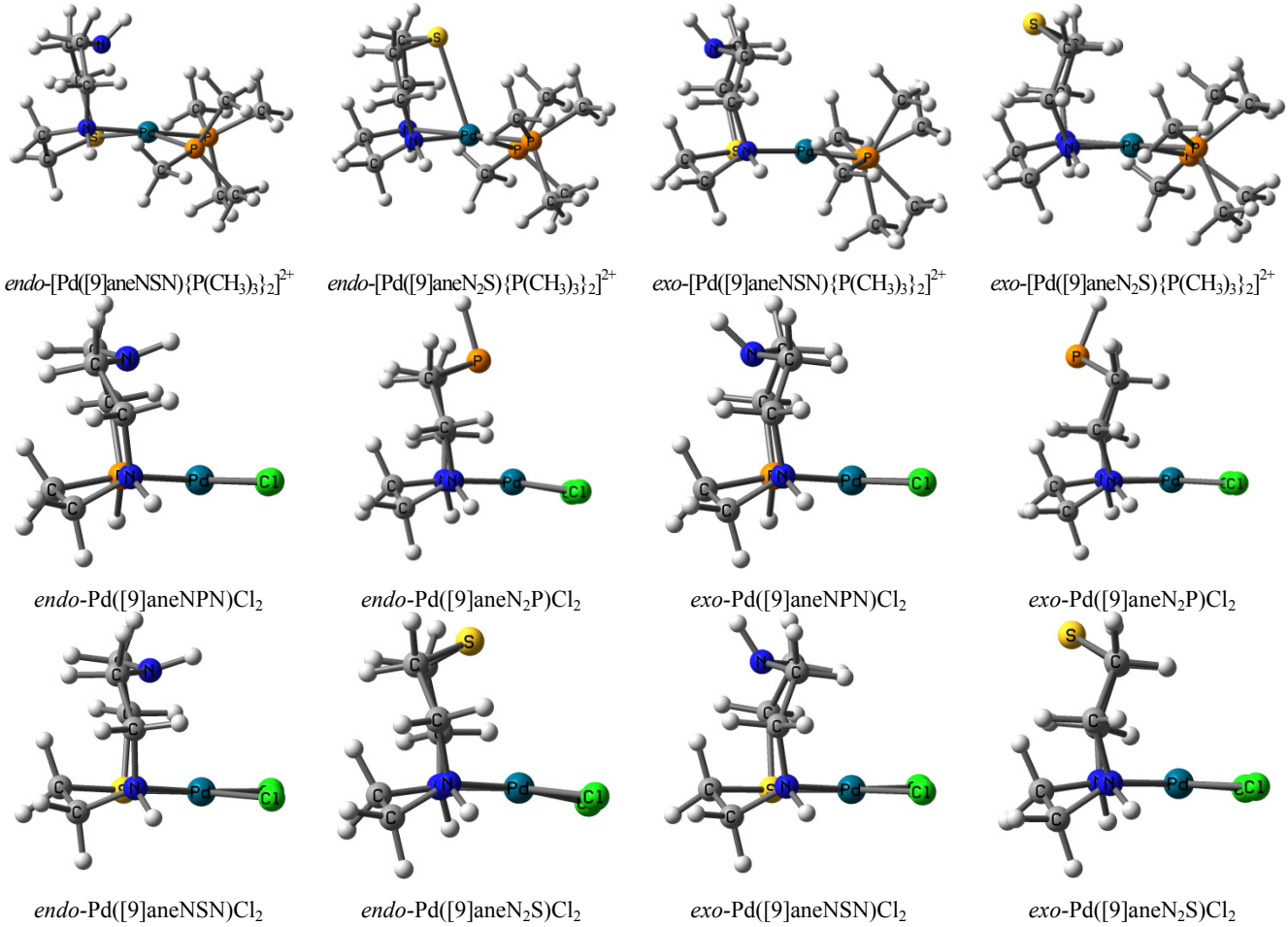

The (soft **A**--Pd) quasi-bond in pentacoordinate *endo*-[Pd([9]ane$\mathbf{B_2A}$)(**L**-donor)$_2$]$^{2+}$ complex causes an isomer of that complex to be more stable than tetracoordinate *endo*-[Pd([9]ane**BAB**)(**L**-donor)$_2$]$^{2+}$ complex {$\Delta E_{BAB\text{-}B2A}$ = 0.10 ~ 0.37 eV for *endo*-[Pd([9]aneN$_2$P)(**L**-donor)$_2$]$^{2+}$, $\Delta E_{BAB\text{-}B2A}$ = 0.08 ~ 0.35 eV for *endo*-[Pd([9]aneN$_2$S) (**L**-donor)$_2$]$^{2+}$}. The relative energy of *endo*-[Pd([9]ane$\mathbf{B_2A}$)(**L**-donor)$_2$]$^{2+}$ pentacoordinate ($\Delta E_{exo\text{-}endo}$ = 0.23~0.70 eV) is lower than the corresponding *exo*-type tetracoordinate. Except for these four *endo*-Pd pentacoordinate complexes, the relative energy of *exo*-[Pd([9]ane**BAB**)(**L**-donor)$_2$]$^{2+}$ tetracoordinate is lower than that of *exo*-[Pd([9]ane$\mathbf{B_2A}$)(**L**-donor)$_2$]$^{2+}$ tetracoordinate {$\Delta E_{BAB\text{-}B2A}$ = −0.70 ~ −0.20 eV for *endo*-Pd([9]ane**BAB**)(**L**-donor)$_2$]$^{2+}$}. The relative energy of tetracoordinate [Pd([9]ane**BAB**)Cl$_2$ complex is also lower than that of [Pd([9]ane$\mathbf{B_2A}$)Cl$_2$ {$\Delta E_{BAB\text{-}B2A}$ = −0.35 ~ −0.18 eV for Pd([9]ane**BAB**)**L**$_2$}. Therefore, the axial (soft **A**--Pd) quasi-bond contributes largely to their relative stability. The geometric parameters listed in Table 1 are very similar to the corresponding parameters given in Supplementary Information Tables S2 and S3.

Table 1. Optimized average bond distances (Å), average atomic charges (CHelpG, au), and relative energies (eV) of the equilibrium structures of {Pd([9]ane$\mathbf{B_2A}$)$\mathbf{L_2}$ and Pd([9]ane**BAB**)$\mathbf{L_2}$} at the B3P86/6-311+G** (lanl2DZ for Pd) level.

Compound	Average distance				Average atomic charge				Relative energy		
	$R^a_{Pd\text{-}N}$	$R^a_{Pd\text{-}P}$	$R^b_{Pd\cdots N}$	$R^b_{Pd\cdots P}$	Q^c_{Pd}	Q^c_{PH3}	Q^d_N	Q^d_P	$\Delta E^e_{H\text{-}L}$	$\Delta E^f_{BAB\text{-}B2A}$	$\Delta E^g_{exo\text{-}endo}$
endo-[Pd([9]aneNPN)$(PH_3)_2$]$^{2+}$	2.195	2.289	2.848		0.348	0.368	−0.151		3.45	0.37	0.00
exptl		2.3214[h]	2.298[i] 2.3207[i]								
endo-[Pd([9]aneN_2P)$(PH_3)_2$]$^{2+}$	2.142			2.782	0.225	0.412		−0.289	2.68	0.00	0.00
theo		2.340[j]			0.598[k]	0.150[k]					
exptl		2.3337[i]									
exo-[Pd([9]aneNPN)$(PH_3)_2$]$^{2+}$	2.154	2.363	3.504		0.405	0.380	−0.152		3.39	−0.70	−0.37
exo-[Pd([9]aneN_2P)$(PH_3)_2$]$^{2+}$	2.129			3.963	0.263	0.449		−0.018	2.74	0.00	0.70
	$R^a_{Pd\text{-}N}$	$R^a_{Pd\text{-}S}$	$R^b_{Pd\cdots N}$	$R^b_{Pd\cdots S}$	Q^c_{Pd}	Q^c_{PH3}	Q^d_N	Q^d_S			
endo-Pd([9]aneNSN)$(PH_3)_2$]$^{2+}$	2.155	2.359	2.720		0.332	0.377	−0.159		3.40	0.10	0.00
endo-[Pd([9]aneN_2S)$(PH_3)_2$]$^{2+}$	2.138			2.877	0.294	0.447		−0.269	2.67	0.00	0.00
exo-[Pd([9]aneNSN)$(PH_3)_2$]$^{2+}$	2.135	2.382	3.602		0.435	0.366	−0.112		2.87	−0.25	−0.03
exo-[Pd([9]aneN_2S)$(PH_3)_2$]$^{2+}$	2.127			3.954	0.343	0.444		−0.033	2.42	0.00	0.32
	$R^a_{Pd\text{-}N}$	$R^a_{Pd\text{-}P}$	$R^b_{Pd\cdots N}$	$R^b_{Pd\cdots P}$	Q^c_{Pd}	$Q^c_{P(CH3)3}$	Q^d_N	Q^d_P	$\Delta E^e_{H\text{-}L}$	$\Delta E^f_{BAB\text{-}B2A}$	$\Delta E^g_{exo\text{-}endo}$
endo-[Pd([9]aneNPN)$\{P(CH_3)_3\}_2$]$^{2+}$	2.214	2.324	3.076		0.464	0.425	−0.133		4.01	0.35	0.00
endo-[Pd([9]aneN_2P)$\{P(CH_3)_3\}_2$]$^{2+}$	2.195			2.843	0.380	0.389		−0.416	3.51	0.00	0.00
exo-[Pd([9]aneNPN)$\{P(CH_3)_3\}_2$]$^{2+}$	2.188	2.368	3.678		0.575	0.439	0.048		3.85	−0.51	−0.28
exo-[Pd([9]aneN_2P)$\{P(CH_3)_3\}_2$]$^{2+}$	2.178			4.049	0.414	0.372		−0.061	3.52	0.00	0.58
	$R^a_{Pd\text{-}N}$	$R^a_{Pd\text{-}S}$	$R^b_{Pd\cdots N}$	$R^b_{Pd\cdots S}$	Q^c_{Pd}	$Q^c_{P(CH3)3}$	Q^d_N	Q^d_S			
endo-Pd([9]aneNSN)$\{P(CH_3)_3\}_2$]$^{2+}$	2.185	2.402	2.920		0.409	-0.392	−0.118		3.88	0.08	0.00
endo-[Pd([9]aneN_2S)$\{P(CH_3)_3\}_2$]$^{2+}$	2.194			2.935	0.353	-0.396		−0.300	3.50	0.00	0.00
exo-[Pd([9]aneNSN)$\{P(CH_3)_3\}_2$]$^{2+}$	2.179	2.420	3.705		0.434	-0.352	0.129		3.55	−0.20	−0.05
exo-[Pd([9]aneN_2S)$\{P(CH_3)_3\}_2$]$^{2+}$	2.176			4.037	0.458	-0.412		−0.107	3.19	0.00	0.23

Table 1. *Cont.*

Compound	Average distance				Average atomic charge				Relative energy		
	R^a_{Pd-N}	R^a_{Pd-P}	$R^b_{Pd\cdots N}$	$R^b_{Pd\cdots P}$	Q^c_{Pd}	Q^c_{Cl}	Q^d_N	Q^d_P	ΔE^e_{H-L}	$\Delta E^f_{BAB-B2A}$	$\Delta E^g_{exo-endo}$
endo-Pd([9]aneNPN)Cl_2	2.113	2.225	3.040		0.801	−0.746	−0.077		4.04	−0.28	0.00
exptl	2.115[l] 2.117[l]	2.3337[i]									
endo-Pd([9]aneN_2P)Cl_2	2.088			3.033	0.720	−0.740		−0.357	3.84	0.00	0.00
theo	2.101[k] 2.049[k]				0.628[k]	−0.516[k]					
exptl	2.0410[i] 2.0354[i]										
exo-Pd([9]aneNPN)Cl_2	2.106	2.346	3.471		0.920	−0.762	−0.086		4.08	−0.35	−0.13
exo-Pd([9]aneN_2P)Cl_2	2.095			3.868	0.695	−0.708		−0.152	4.03	0.00	−0.06
	R^a_{Pd-N}	R^a_{Pd-S}	$R^b_{Pd\cdots N}$	$R^b_{Pd\cdots S}$	Q^c_{Pd}	Q^c_{Cl}	Q^d_N	Q^d_S			
endo-Pd([9]aneNSN)Cl_2	2.094	2.324	2.923		0.771	−0.747	−0.073		3.73	-0.18	0.00
exptl	2.124[m]	2.2492[m] 2.332[n]	2.638[m]								
endo-Pd([9]aneN_2S)Cl_2	2.091			3.190	0.609	−0.722		−0.304	3.77	0.00	0.00
exptl	2.077[m] 2.117[o] 2.144[o]			3.0865[m] 3.293[o]							
exo-Pd([9]aneNSN)Cl_2	2.094	2.329	3.465		0.787	−0.727	0.076		3.85	−0.21	−0.13
exptl	2.068[p] 2.050[p]	2.2685[m] 2.317[q]	3.499[p]								
exo-Pd([9]aneN_2S)Cl_2	2.094			3.854	0.774	−0.724		−0.178	4.04	0.00	−0.09

[a]Bond length between the Pd^{II} center and equatorial binding site of the tridentate ligand; [b]Bond length between the Pd^{II} center and axial binding site of the tridentate; [c]Atomic charges of the Pd^{II} center and the binding atom of *trans* **L**-donor; [d]Atomic charge of the apical binding atom; [e]Energy gap between HOMO and LUMO; [f]Relative energy gap between Pd([9]ane**BAB**)$\mathbf{L}_2$ and Pd([9]ane$\mathbf{B_2A}$)$\mathbf{L}_2$; [g]Energy gap between *exo*- and *endo*-type structures; [h]Ref. [23]; [i]Ref. [42]; [j]Ref. [17]; [k]Ref. [44]; [l]Ref. [18]; [m]Ref. [40]; [n]Ref. [53]; [o]Ref. [41]; [p]Ref. [37]; [q]Ref. [54].

In previous studies [18–36], unusual penta-, hexa-, and octacoordinate Pd complexes with some apical (**A**-Pd) bonds were synthesized under some restrictions such as electronic effect of the strong σ-donor in an electron-rich *trans* **L**-ligand and steric effect of the bulky ligand. In the Pd-mediated cross-coupling reactions of an allylic group, the geometry of the (allyl)Pd$\mathbf{L}_2$ crystals was observed to be distorted penta- and hexacoordinate structures [18–24]. Three carbons of an allylic group (η^3-C_3H_5) are axially coordinated to the Pd center of the $Pd^{(0)}\mathbf{L}_n$ precursor. The average distances of the apical (allyl-Pd) bond are short ($R_{C\text{-}Pd}$ = 2.101~2.253 Å) [18,19,22,23]. Interestingly, in the aza-macrocyclic $Pd^{(0)}(C_{10}H_{16}N_2Me_2)$ complexes [33–35] and macrocyclic Pd**L** complexes where **L** = *1,4a,5,8a*-tetra-hydronaphthalene-2,6-dione [36], the six and eight coordination bonds of the 3~4 olefin units with Pd were formed by the steric effect of the bulky ligand. Due to the steric hindrance, none of these three carbons of the olefin units was positioned at the edge of the formal geometry (*i.e.*, the trigonal bipyramid or square pyramid) [18–29]. Furthermore, in the (olefin)Pd$\mathbf{L}_2$ complex with an apical olefin-Pd bond, various (olefin)Pd$\mathbf{L}_2$ intermediates were observed during the Pd-mediated cross-coupling reactions [20,25,26,30]. However, in $[Pd([9]ane\mathbf{N}_3)_2]^{2+}$ and $[Pd([9]ane\mathbf{N}_3)_2(H[9]ane\mathbf{N}_3)_2]^{3+}$ complexes without geometric constraints, the structures with an apical (soft **A**…Pd) interaction were not observed [40].

As shown in Figure 2, when the soft **A** and hard **B** binding sites simultaneously coordinate to the $4d_{x2-y2}$ orbital, the large σ-donor of the **A** site overlaps more with the $4d_{x2-y2}$ orbital than the small σ-donor of **B**. With increasing atomic size (P:107 pm ≅ S:105 pm >> N:71 pm) [52], the larger σ-orbital of the soft **A** site in [9]ane**BAB** first interacts with the $4d_{x2-y2}$ orbital on the square-planar plane. In *endo*-Pd([9]ane**BAB**)$\mathbf{L}_2$ of **(f)** of Figure 2, due to its atomic size, the bond length (r_{Pd-P} = 2.324 ~ 2.225 Å and r_{Pd-S} = 2.402 ~ 2.324 Å) of the equatorial (A-Pd) bond is longer than the corresponding (N-Pd) bond (r_{Pd-N} = 2.214 ~ 2.094 Å). Two equatorial bond lengths (r_{Pd-A}, r_{Pd-B}) are unsymmetrical in nature. The axial distance between the axial **N** site and Pd^{II} center is long (r_{Pd-N} = 2.720 ~ 3.076 Å). As shown in **(g)** of Figure 2, in the *endo*-$[Pd([9]ane\mathbf{B}_2\mathbf{A})(\mathbf{L}\text{-donor})_2]^{2+}$ complex, the average distance between the equatorial **N** site and Pd^{II} center is short (R_{Pd-N} = 2.138 ~ 2.195 Å). Because both the equatorial (**N**-Pd) bonds are short, the large σ-donor of the apical **A** site closely approaches to the Pd center. Thus, the large σ-donor of the soft **A** site can interact with the low-lying unoccupied a_{1g}(5s)-orbital of Pd$\mathbf{L}_2$ complex.

The ratio of products in Pd-catalyzed cross-coupling reactions was experimentally determined by the strength of the σ-donor ligand (e.g., *n*-Bu_3N or an acetate anion) [6,30,31]. As the softness (P ≅ S > N) [47] and basicity (N > P > S) [6,26] of the binding site increases, the coordination bond of the soft **A** site to the $4d_{x2-y2}$-orbital was more preferred than that of the hard **B** site. That is, the σ-donor of the soft **A** site demonstrates a stronger overlap on the $4d_{x2-y2}$ orbital than the hard **B** site. As shown in Table 1, *exo*-$[Pd([9]ane\mathbf{BAB})(\mathbf{L}\text{-donor})_2]^{2+}$ and Pd([9]ane**BAB**)Cl_2 complexes with an equatorial (**A**-Pd) bond are more stable than the corresponding *exo*-$[Pd([9]ane\mathbf{B_2A})(\mathbf{L}\text{-donor})_2]^{2+}$ and Pd([9]ane$\mathbf{B_2A}$)Cl_2 isomers without the equatorial (**A**-Pd) bond, respectively. As described in Supplementary Information Figure **S1** and Table **S1**, *endo*-$[Pd([9]ane\mathbf{PNP})(\mathbf{L}\text{-donor})_2]^{2+}$ could not be optimized. By strong softness and basicity of the binding **A** site, the relative energy of tetracoordinate *endo*-$[Pd([9]ane\mathbf{A_2B})(\mathbf{L}\text{-donor})_2]^{2+}$ complex with two equatorial (**A**-Pd) bonds is lower than that of pentacoordinate *endo*-$[Pd([9]ane\mathbf{ABA})(\mathbf{L}\text{-donor})_2]^{2+}$ complex with an axial (**A**-Pd) bond

{$\Delta E_{BAB\text{-}B2A}$ = −0.01 ~ −0.02 eV for *endo*-Pd([9]aneS_2N)(**L**-donor)$_2$]$^{2+}$}. However, in the *endo*-[Pd([9]ane$\mathbf{B_2A}$)(**L**-donor)$_2$]$^{2+}$ complex with an axial fifth (**A**--Pd) quasi-bond, the pentacoordinate Pd complex is more stable than the tetracoordinate *endo*-[Pd([9]ane**BAB**)(**L**-donor)$_2$]$^{2+}$ complexes. Therefore, in case of interaction of [9]ane$\mathbf{B_2A}$ to Pd$\mathbf{L_2}$, the relative stability of the Pd complexes and the selective formation of the coordination bond may depend on the ***strength*** of the hardness/softness and basicity of **A** (or **B**) and the ***position*** of the equatorial (or apical) binding atoms, and the ***existence*** of an axial (**A**--Pd) quasi-bond [6,26,30,31,47,55].

Figure 2. The equatorial coordination bonds of the **A** (or **B**) site to the $4d_{x^2-y^2}$-orbital and the axial (**A**…Pd) interaction in the *endo*-Pd([9]ane$\mathbf{B_2A}$)$\mathbf{L_2}$ complexes.

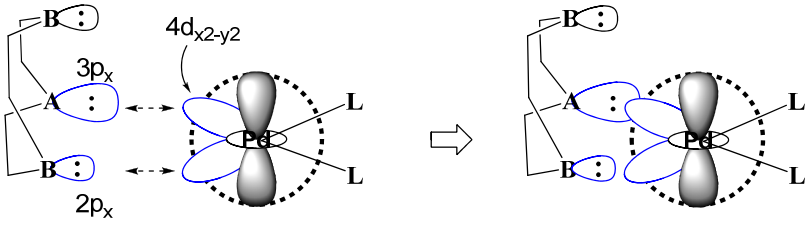

endo-Pd([9]ane**BAB**)$\mathbf{L_2}$, **(f)**

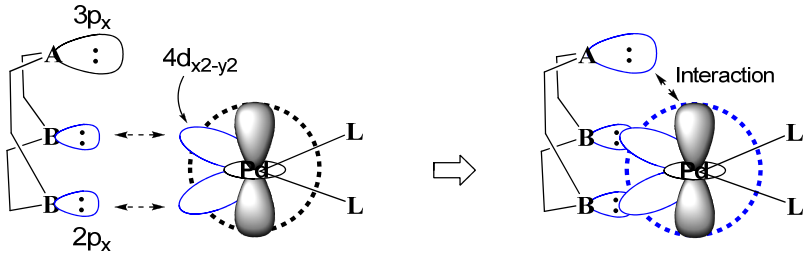

endo-Pd([9]ane$\mathbf{B_2A}$)$\mathbf{L_2}$, **(g)**

In some Pd^{II} complexes with terminal amino derivatives [37–42], both apical soft **S**…Pd and hard **N**…Pd interactions were observed under the strong strain of a polymeric side chain. In particular, the apical (hard **N**…Pd) distances ($r_{Pd\cdots N}$ = 2.523 ~ 2.638 Å) [40] are slightly shorter as explained by an axial σ*…d_{z2} interaction between an antibonding orbital of the apical N site and the filled d_{z2}-orbital [42]. Meanwhile, in the ligand exchange processes of the Pd complexes [46,47], an axial water…Pd interaction was also observed. The mechanism of the hydration reactions is described by two models: axial H_2O…d_z^2-orbital and OH_2…d_z^2-orbital interactions with the former being rarely formed due to electrostatic repulsions. In studies by Kozelka *et al.* [56], both the axial O_2H…Pt and H_2O…Pt interactions in the Pt complex were explained by an electrostatic attraction between the dispersion components. Until now, the axial **L**…d^8-metal interaction between the axial **L**-ligand and d^8-metal have not been explained in detail using an orbital interaction.

The $3a_{1g}$(5s)-orbital [(**h**), (**j**), (**l**)] and the $2a_{1g}$-orbital [(**i**), (**k**), (**m**)] of *endo*-Pd complexes are illustrated in Figure 3. As shown in **(h)**, **(j)**, and **(l)** of Figure 3, the orbital shape of the $3a_{1g}$(5s)-orbital of the *endo*-Pd([9]ane$\mathbf{B_2A}$)$\mathbf{L_2}$ complexes is largely varied by the donating (or withdrawing) property of the *trans* **L**-ligand. Due to the electron donating property of *trans* **L**-donor, its electron density moves to the Pd^{II} center, and then the increased electron density at the Pd^{II} center is transferred to the low-lying unoccupied $3a_{1g}$(5s)-orbital. The orbital lobe of the $3a_{1g}$(5s)-orbital around the Pd^{II} center is huge

[as shown in tetracoordinate *endo*-[Pd([9]ane**BAB**)(**L**-donor)$_2$]$^{2+}$ complex of **(h)** and **(j)** of Figure **3**]. This huge lobe of the 3a$_{1g}$(5s)-orbital can interact with the σ-donor of the soft **A** site [or filled π-donor orbital of substrates]. In the *endo*-[Pd([9]ane**B$_2$A**)(**L**-donor)$_2$]$^{2+}$ complex with an apical (**A**--Pd) quasi-bond [**(h)** and **(j)** of Figure **3**], the shape of the 3a$_{1g}$(5s)-orbital is not symmetric. The partially unfilled and lowered a$_{1g}$(5s)-orbital strongly interacts with the large σ-donor of **A** to make the apical (**A**--Pd) quasi-bond. The upper part of the a$_{1g}$(5s)-orbital lobe is used for the apical (**A**···Pd) interaction. Meanwhile, in the *endo*-[Pd([9]ane**BAB**)(**L**-donor)$_2$]$^{2+}$ complex without the apical (**A**--Pd) quasi-bond [**(h)** and **(j)** of Figure 3], the orbital lobe of the 3a$_{1g}$(5s)-orbital is huge and symmetric. The 3a$_{1g}$(5s)-orbital of *endo*-[Pd([9]ane**BAB**)(**L**-donor)$_2$]$^{2+}$ complex is quite different from that of *endo*-[Pd([9]ane**B$_2$A**)(**L**-donor)$_2$]$^{2+}$. As shown in **(l)** of Figure 3 with *trans* Cl-acceptor, the lobe size of the 3a$_{1g}$(5s)-orbital is very small. No interaction between the σ-donor of the soft **A** site and the 3a$_{1g}$(5s)-orbital is formed. The orbital shapes of the 3a$_{1g}$(5s)-orbital and the 2a$_{1g}$-orbital are very similar to those given in Supplementary Information Figures **S2** and **S3**. As listed in Table 1, the atomic charge of Pd in [Pd([9]ane**B$_2$A**)(**L**-donor)$_2$]$^{2+}$ complex is more negative than that of Pd in Pd([9]ane**B$_2$A**)Cl$_2$ complex.

Figure 3. The 3a$_{1g}$(5s)-orbital [(**h**), (**j**), (**l**)] and 2a$_{1g}$-orbital [(**i**), (**k**), (**m**)] of *endo*-Pd([9]ane**B$_2$A**)**L**$_2$ and *endo*-Pd([9]ane**BAB**)**L**$_2$ complexes calculated at the B3P86/6-311+G** (lanl2DZ for Pd) level, respectively.

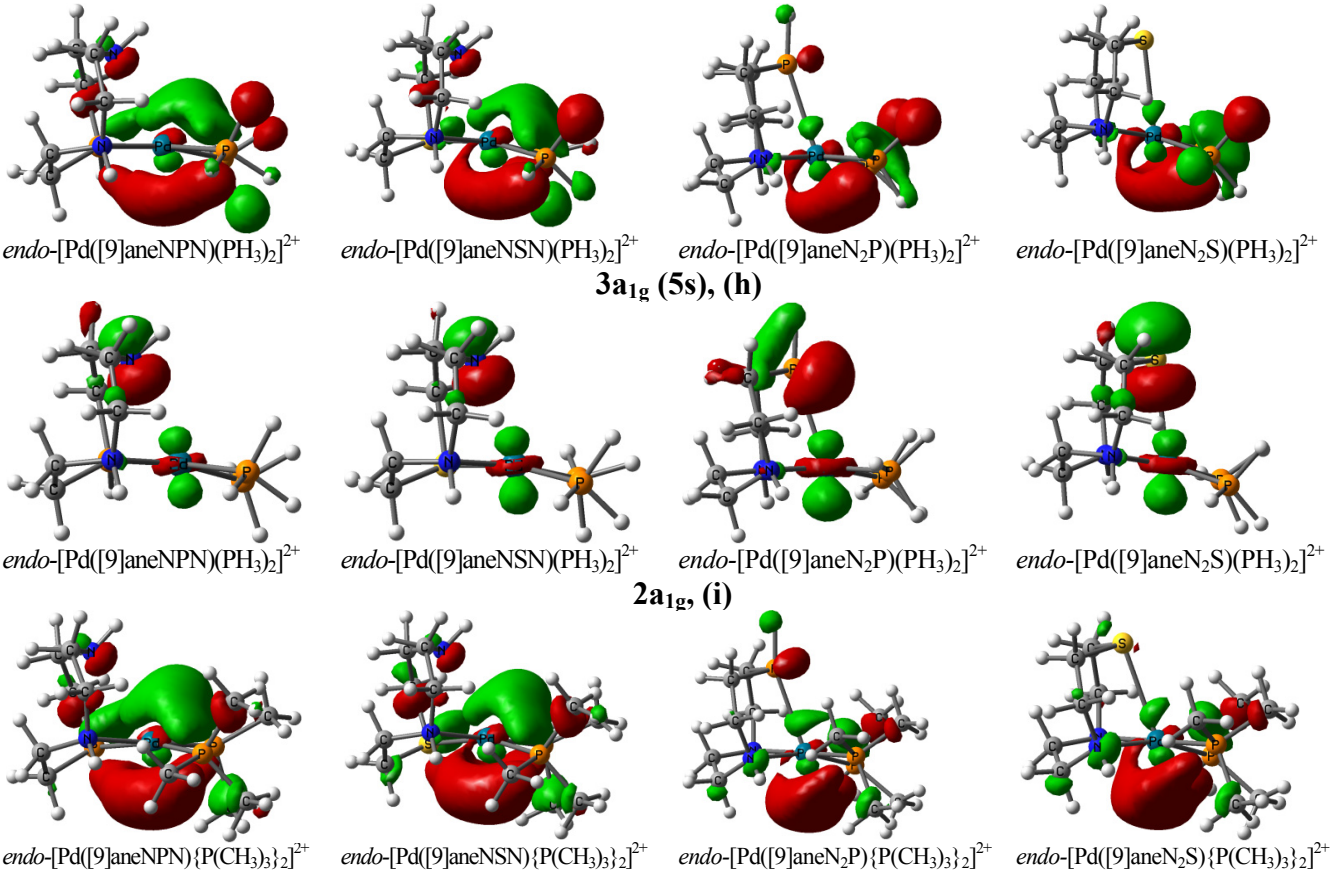

Figure 3. *Cont.*

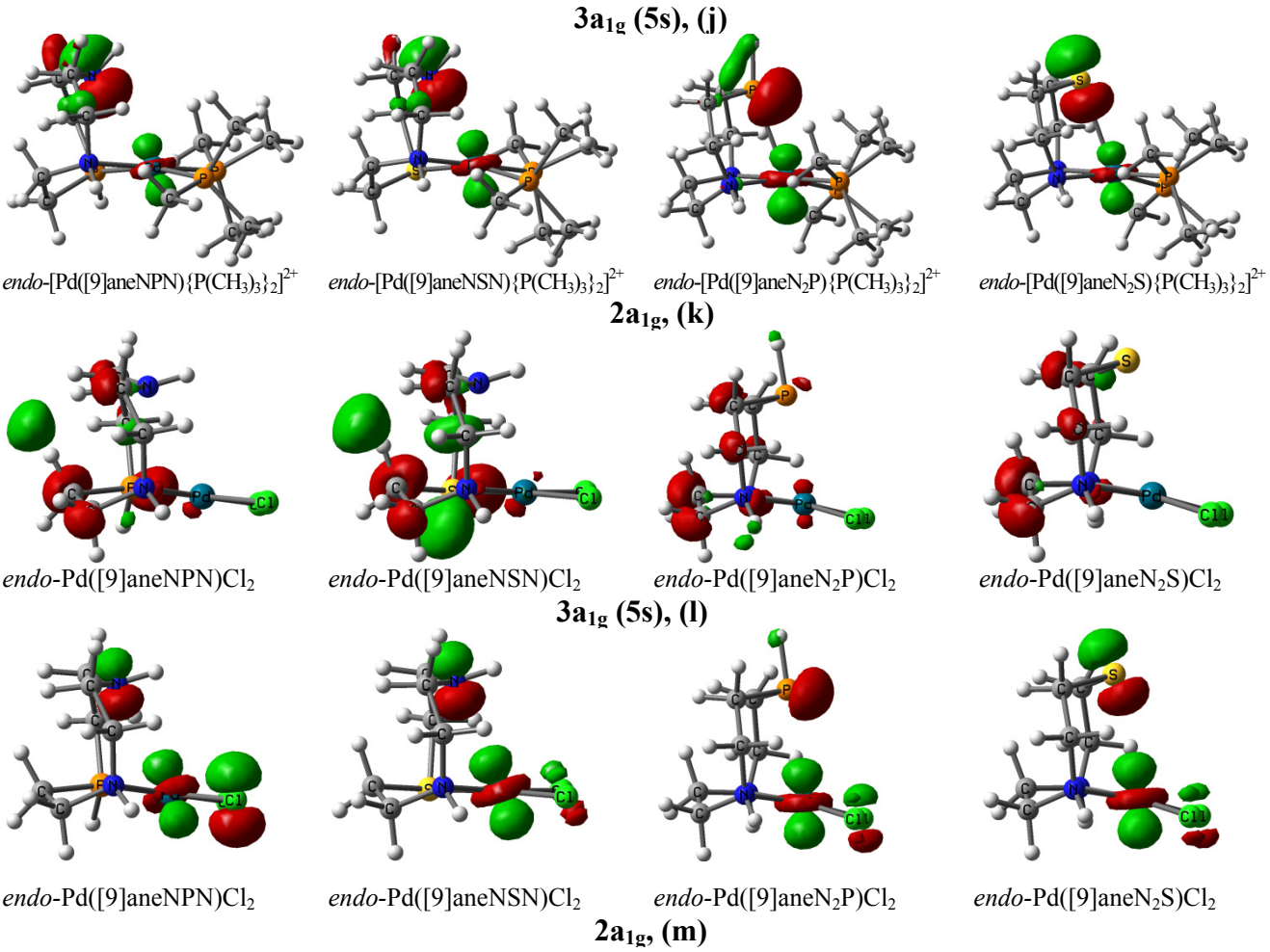

Based on Figure 3, orbital interaction between the σ-donor of the apical soft **A** (or hard **B**) site and the partially unfilled $a_{1g}(5s)$-orbital of Pd^{II} center as well as the direction for the electron transfer of *trans* **L**-ligand (electron-donor or acceptor) are schematically depicted in Figure 4. In *endo*-[Pd([9]ane$\mathbf{B_2A}$)(**L**-donor)$_2$]$^{2+}$ and *endo*-[Pd([9]ane**BAB**)(**L**-donor)$_2$]$^{2+}$ complexes, the electron density of the unfilled $a_{1g}(5s)$-orbital of Pd^{II} center is greatly increased by the strong electron-donating property of the *trans* **L**-donor. The spatial distribution of electron density of the $a_{1g}(5s)$-orbital is larger than that of the $a_{1g}(4d_z^2)$-orbital, thus positioning the lobe of $a_{1g}(5s)$-orbital at the outer space of the $a_{1g}(4d_z^2)$-orbital. As represented in **(n)** of Figure 4, the soft σ-donor of the axial **A** site (or substrate of Lewis base) first interacts with the partially unoccupied $a_{1g}(5s)$-orbital (or Pd-complex of Lewis acid). A fifth apical (soft **A**--Pd) quasi-bond is formed as shown in Figure 1. In **(o)** of Figure 4, the size of σ-donor in an axial **B** site is small [covalent radius of the N atom: 71 pm [52]]. In the regular Pd tetracoordinate, the axially hard **N** atom cannot easily interact with the Pd center. Meanwhile, in *endo*-Pd([9]ane$\mathbf{B_2A}$)Cl_2 and *endo*-Pd([9]ane**BAB**)Cl_2 complexes with a *trans* Cl-acceptor, the filled $a_{1g}(4d_z^2)$-orbital of Pd^{II} center lies spatially outside than that of the $a_{1g}(5s)$-orbital. There is no interaction between the soft σ-donor of **A** and the filled $a_{1g}(4d_z^2)$-orbital.

Figure 4. The axial orbital interaction between the σ-donor of the soft **A** site (or hard **B** site) and the partially unfilled a_{1g}(5s)-orbital is influenced by the electronic property of the *trans* **L**-ligand and the size of the σ-donor of **A** (or **B**).

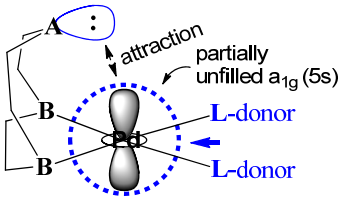

endo-[Pd([9]ane**B**$_2$**A**)(**L**-donor)$_2$]$^{2+}$, **(n)**

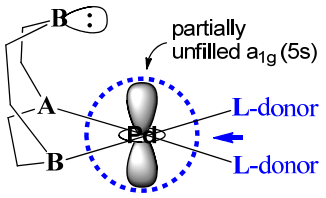

endo-[Pd([9]ane**BAB**)(**L**-donor)$_2$]$^{2+}$, **(o)**

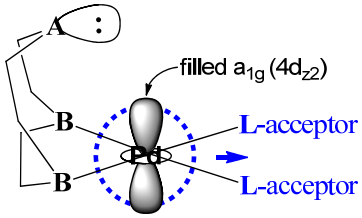

endo-Pd([9]ane**B**$_2$**A**)Cl$_2$, **(p)**

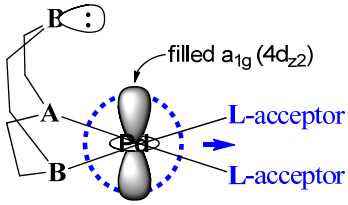

endo-Pd([9]ane**BAB**)Cl$_2$, **(q)**

Experiments to analyze the electronic effect of a donating (or withdrawing) Z group were performed by some research groups [30,31]. The results of these experiments indicated that the rate of catalytic activity of the neutral Pd^0(dba-*n,n'*-Z)$_2$ precursor is greatly dependent on the electronic property (donor or acceptor) of the bulky dba-*n,n'*-Z ligand. Owing to the increase in the strength of electron donating dba-*n,n'*-Z ligand, the overall rate of the oxidative addition of phenyl iodide to Pd^0(dba-*n,n'*-Z)$_2$ precusor is faster than that of the Pd^0 complex with an electron withdrawing Z group. In particular, the rate of oxidative addition of aryl halide to Pd^0**L**$_n$ depends on the concentration of the active Pd^0**L**$_n$ precursor with a strong electron-donating *trans* **L**-ligand. Scrivanti *et al.* [38,39] found that the rate of oxidative addition of an aryl halide to the (iminophosphine)Pd^0(η^2-olefin) complex also increased. The increase in reaction rate is explained by the catalyst stability of the moderate π-accepting ligand. These experimental results [31,39] showing an increased rate in the catalytic activity may have originated from the electronic property of a strong electron-donating *trans* **L**-ligand in Pd^0**L**$_n$. Based on Figures 3 and 4, in the oxidative addition of ArX to Pd^0**L**$_n$, the donating π-orbital of the aryl halide can interact with the low-lying unfilled a_{2u}(5p)-orbital of Pd. Thus, an a_{2u}(5p)⋯π-orbital interaction between the low-lying unfilled a_{2u}(5p)-orbital of Pd and the filled π-orbital of ArX can take place. These experimental results can be understood with the help of results shown in Figure 3.

The orbital energy levels for the orbital interaction associated with the coordination bond of [9]ane**B**$_2$**A** to Pd**L**$_2$ are drawn in Figure 5. As shown in **(r)** of Figure **5**, there is a large gap in the energy level between the **A** site of [9]ane**B**$_2$**A** and the a_{1g}(5s)-orbital of Pd**L**$_2$. Therefore, the σ-orbital of **A** cannot easily interact with the unoccupied a_{1g}(5s)-orbital. Meanwhile, as shown in **(s)** of Figure **5**, the energy gap between the axial **A** site and a_{1g}(5s)-orbital is largely reduced. In the *endo*-[Pd([9]ane**BAB**)(**L**-donor)$_2$]$^{2+}$ complex as shown in **(h)** and **(j)** of Figure **3**, the unoccupied $3a_{1g}$(5s)-orbital is partially filled by the electron density transfer from *trans* **L**-donor and ***the level of the partially filled 3a$_{1g}$(5s)-orbital decreases.*** In *endo*-[Pd([9]ane**B**$_2$**A**)(**L**-donor)$_2$]$^{2+}$ complex as shown in **(i)** and **(k)** of Figure **3**, the huge σ-orbital of the soft **A** site can overlap with the partially filled $3a_{1g}$(5s)-orbital and then ***the energy level of the A site is increased*** by the [σ-donor ↔ $3a_{1g}$(5s)]

overlap. Therefore, the electron density of increased energy level in σ-orbital of **A** can share with that of the decreased energy level of $3a_{1g}$(5s)-orbital. The unfilled $3a_{1g}$-molecular orbital is occupied and the energy level is largely lowered as HOMO. The energy difference between the HOMO and LUMO is also reduced {$\Delta E2_{H\text{-}L}$ = 2.67~3.51 eV for *endo*-[Pd([9]ane$\mathbf{B_2A}$)(**L**-donor)$_2$]$^{2+}$}. As shown in **(t)** of Figure **5**, the orbital energy levels are similar to that in **(r)** of Figure **5**. The σ-orbital cannot interact with the $3a_{1g}$(5s)-orbital and the energy gap between the HOMO and LUMO is large {$\Delta E1_{H\text{-}L}$ = 3.77 and 3.84 eV for *endo*-Pd([9]ane$\mathbf{B_2A}$)Cl_2}.

Similar to the interaction suggested above [σ-donor···unfilled a_{1g}(5s)], the fifth [sixth, eighth] axial olefin-Pd coordination bond in the oxidative addition of olefin to $Pd^{(0)}\mathbf{L}_n$ can be formed by an axial π-donor···unfilled $a_{2u}(5p_{x,y})$ interaction between the π-donor of olefin and an unfilled $a_{2u}(5p_{x,y})$-orbital of Pd. The electron density transfer from the *trans* **L**-donor to the unfilled $a_{2u}(5p_{x,y})$-orbital makes it partially occupied, and thus the energy level of the partially unfilled $a_{2u}(5p_{x,y})$-orbital is lowered. Consequently, the π-donor electron-rich substrates such as olefin can interact with the partially unfilled and lowered $a_{2u}(5p_{x,y})$-orbital of Pd. In the Pd-mediated cross-coupling reactions, the results of this study can describe the mechanism for the formation of the apical σ-donor···unfilled a_{1g}(5s) and π-donor···unfilled $a_{2u}(5p_{x,y})$ interactions in ArPd$\mathbf{L}_n$X. Furthermore, in d^9-electron systems such as $[Cu(NH_3)_4(H_2O)_2]^{2+}$ [57,58], a distorted octahedron with two water molecules at a longer distance than four ammonias is formed *via* the long range interactions. The vertical Cu-OH_2 bond length ($R_{Cu\text{-}O}$ = 2.204 Å) is longer than that ($R_{Cu\text{-}N}$ = 1.933 Å) of the equatorial Cu-NH_3 bond [55]. The two longer Cu-OH_2 bonds along the z-axis are explained by the interaction between the half unoccupied $3d_{z2}$-orbital of Cu^{II} and the filled σ-orbital of the oxygen atom in water.

The relative energies through the structural variation from *endo*-Pd([9]ane$\mathbf{B_2A}$)$\mathbf{L}_2$ complex to *endo*-Pd([9]ane**BAB**)$\mathbf{L}_2$ are represented in Figure 6. In the **(u)** reaction path, the relative energy level of *endo*-[Pd([9]ane$\mathbf{B_2A}$)(**L**-donor)$_2$]$^{2+}$ complex with the fifth (**A**--Pd) quasi-bond is lower than that of *endo*-[Pd([9]ane**BAB**)(**L**-donor)$_2$]$^{2+}$ {$\Delta E_{BAB\text{-}B2A}$ = −0.37, −0.10, −0.35, and −0.08 eV for *endo*-[Pd([9]ane$\mathbf{B_2A}$)(**L**-donor)$_2$]$^{2+}$}. The axial (**A**--Pd) quasi-bond greatly contributes to the relative stability of the pentacoordinate *endo*-[Pd([9]ane$\mathbf{B_2A}$)(**L**-donor)$_2$]$^{2+}$ complexes. In the **(v)** reaction path, the relative energy level of *endo*-Pd([9]ane**BAB**)Cl_2 {*endo*-Pd([9]ane$\mathbf{A_2B}$)Cl_2} complex is more stable than that of *endo*-Pd([9]ane$\mathbf{B_2A}$)Cl_2 {*endo*-Pd([9]ane**ABA**)Cl_2} complex (ΔE = −0.18~−0.28 eV for *endo*-Pd([9]ane**BAB**)Cl_2). Due to the relative stability between the axial and equatorial (**A**-Pd) bonds, the Pd([9]ane**ABA**)$\mathbf{L}_2$ and Pd([9]ane$\mathbf{A_2B}$)$\mathbf{L}_2$ structures with one or two equatorial (**A**-Pd) bonds are more stable than the Pd([9]ane$\mathbf{B_2A}$)$\mathbf{L}_2$ and Pd([9]ane**BAB**)$\mathbf{L}_2$ structures, respectively (as shown in Table 1 and Supplementary Information Table **S1**). In particular, in the **(w)** reaction path, the geometric configuration of *endo*-[Pd([9]ane**PNP**)(**L**-donor)$_2$]$^{2+}$ automatically optimizes to the *endo*-[Pd([9]ane$\mathbf{P_2N}$)(**L**-donor)$_2$]$^{2+}$ structure without the transition energy barrier. {*endo*-[Pd([9]ane**PNP**)(**L**-donor)$_2$]$^{2+}$ could not be optimized.} Therefore, the relative stability and configurational and conformational changes (such as axial-equatorial coordination and *cis-trans* isomerization) of the $RPd^{II}(\mathbf{L})_nX$ intermediates are largely influenced by the axial (soft **A**···Pd) interaction, relative Pd affinity of the soft **A** atom, and low potential energy barrier.

Figure 5. The variation in the orbital energy levels of *endo*-Pd([9]ane$\mathbf{B_2A}$)$\mathbf{L_2}$ complex, showing the coordination bonds of [9]ane$\mathbf{B_2A}$ to [Pd(**L**-donor)$_2$]$^{2+}$ and [PdCl$_2$]. In *endo*-[Pd([9]ane$\mathbf{B_2A}$)(**L**-donor)$_2$]$^{2+}$ complex **(r)**, the separated configuration of two electron spins filled in the 3a$_{1g}$-orbital indicates the (**A**--Pd) quasi-bond.

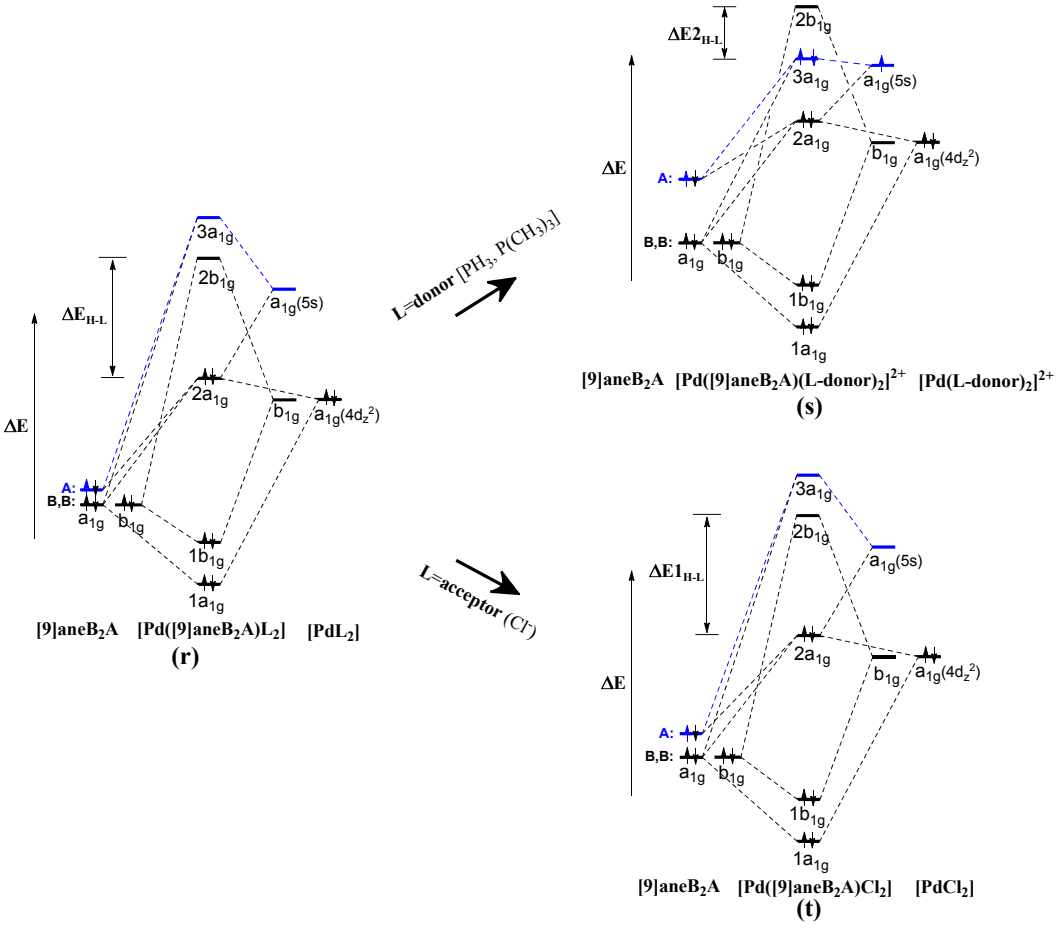

Figure 6. The variation of the structural configuration from *endo*-Pd([9]ane$\mathbf{B_2A}$)$\mathbf{L_2}$ {or *endo*-Pd([9]ane**ABA**)$\mathbf{L_2}$} complex to *endo*-Pd([9]ane**BAB**)$\mathbf{L_2}$ {or *endo*-Pd([9]ane$\mathbf{A_2B}$)$\mathbf{L_2}$} complex, including the relative energy level (**A**:P, S; **B**:N). (**u**) is a reaction path from the pentacoordinate *endo*-[Pd([9]ane$\mathbf{B_2A}$)(**L**-donor)$_2$]$^{2+}$ complex with an axial (soft **A**--Pd) quasi-bond to *endo*-[Pd([9]ane**BAB**)(**L**-donor)$_2$]$^{2+}$. (**v**) is a reaction path from the tetracoordinate *endo*-Pd([9]ane$\mathbf{B_2A}$)(**L**-acceptor)$_2$ complex with a *trans* **L**-acceptor to *endo*-Pd([9]ane**BAB**)(**L**-acceptor)$_2$. (**w**) is a reaction path from the *endo*-Pd([9]ane**PNP**)(**L**-donor)$_2$ complex to *endo*-Pd([9]ane$\mathbf{P_2N}$)(**L**-donor)$_2$ without the transition energy barrier.

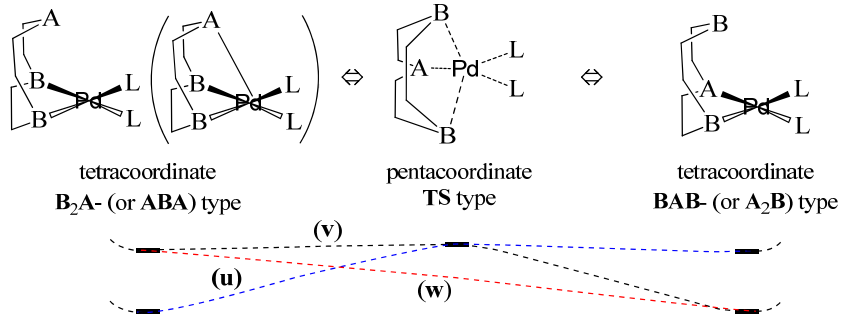

4. Conclusions

We investigated the geometric structures and relative stabilities of Pd([9]ane$\mathbf{B_2A}$)$\mathbf{L_2}$ complexes {Pd([9]ane**BAB**)$\mathbf{L_2}$, *endo*-Pd([9]ane$\mathbf{A_2B}$)$\mathbf{L_2}$, *endo*-Pd([9]ane**ABA**)$\mathbf{L_2}$}, the selective orbital interaction for an axial or equatorial (**A**…Pd) coordination of [9]ane$\mathbf{B_2A}$ with Pd$\mathbf{L_2}$, and the electronic effects of the soft **A**/hard **B** donors and the donating/withdrawing *trans* **L**-ligand. The *endo*-[Pd([9]ane$\mathbf{B_2A}$)(**L**-donor)$_2$]$^{2+}$ complex with an axial (soft **A**--Pd) quasi-bond was optimized as a pentacoordinate geometry, while the other Pd-complexes were optimized as tetracoordinate structures. The relative energy of the pentacoordinate Pd complexes is lower than that of the corresponding *endo*-Pd tetracoordinates. Among the Pd tetracoordinated species, the Pd([9]ane**BAB**)$\mathbf{L_2}$ structure with an equatorial (soft **A**-Pd) bond is more stable than the Pd([9]ane$\mathbf{B_2A}$)$\mathbf{L_2}$ type with both the equatorial (hard **B**-Pd) bonds. Furthermore, the *endo*-[Pd([9]ane$\mathbf{A_2B}$)(**L**-donor)$_2$]$^{2+}$ tetracoordinated with two equatorial (**A**-Pd) bonds is more stable than pentacoordinated *endo*-[Pd([9]ane**ABA**)(**L**-donor)$_2$]$^{2+}$. And the *endo*-[Pd([9]ane**PNP**)(**L**-donor)$_2$]$^{2+}$ type of structures is automatically optimized to the stable *endo*-[Pd([9]ane$\mathbf{P_2N}$)(**L**-donor)$_2$]$^{2+}$ type of structures. The relative stability of the Pd-complexes and the equatorial or axial selectivity of the soft **A**/hard **B** donors to Pd^{II} center are dependent upon its softness, basicity, and electronic effects.

In the Pd-catalyzed coupling reactions, the Pd$\mathbf{L_n}$ intermediates are activated by an electron-rich *trans* **L**-donor possessing a strong Lewis base character. The strong Lewis base character of the *trans* **L**-donor allows its electron density to transfer to the low-lying unoccupied orbitals [a_{1g}(5s) or a_{2u}(5p)] of Pd and the energy level of the partially unfilled a_{1g}(5s)-orbital of Pd is decreased. Therefore, an axially fifth substrate···Pd$\mathbf{L_2}$ interaction between the σ(or π)-donor of substrates (such as hemilabile multidentates, olefinic halides, and solvents) and the Pd$\mathbf{L_2}$ precursor should occur energetically, resulting in the electronic and steric effects of the bulky and electron-rich ligand. Because of the low transition barrier and an axial substrate···Pd$\mathbf{L_2}$ interaction, the configurational and conformational changes of $RPd^{II}(\mathbf{L})_nX$ can easily take place (e.g., axial-equatorial and *cis-trans* exchanges and interconversions in $RPd^{II}(\mathbf{L})_nX$ intermediates). Consequently, the geometric structure and relative stability of the Pd complexes are influenced by the relative strength of the axial or equatorial (soft **A**···Pd) interaction, donating electron property of the *trans* **L**-ligand, and relative Pd affinity of the **A** and **B** donors. The mechanisms for orbital interaction and electron density transfer proposed in this study can be considerably valuable in the design of useful Pd-catalyst and synthetic applications for the Pd-catalyzed cross-couplings of substrates.

Supplementary Materials

Supplementary materials can be accessed at: http://www.mdpi.com/1420-3049/18/10/12687/s1.

Acknowledgments

We gratefully acknowledge the support of Chemistry Research Fund of Gyeongsang National University. This work was supported by the fund of Research Promotion Program (RPP-2010-018), Gyeongsang National University.

Conflicts of Interest

The authors declare no conflict of interest.

References

1. Amatore, C.; Jutand, A. *Handbook of Organopalladium Chemistry for Organic Synthesis*; John Wiley and Sons: New York, NY, USA, 2002; Volume 1, p. 943.
2. De Meijere, A.; Diederich, F. *Metal Catalyzed Cross Coupling Reactions*, 2nd ed.; John Wiley and Sons: New York, NY, USA, 2004; Volumes1 and 2.
3. Amatore, C.; Jutand, A. Anionic Pd(0) and Pd(II) Intermediates in Palladium-Catalyzed Heck and Cross-Coupling Reactions. *Acc. Chem. Res*. **2000**, *33*, 314–321.
4. Littke, A.F.; Fu, G.C. Palladium-catalyzed coupling reactions of aryl chlorides. *Angew. Chem. Int. Ed*. **2002**, *41*, 4176–4211.
5. Grushin, V.V. Mixed Phosphine-Phosphine Oxide Ligands. *Chem. Rev.* **2004**, *104*, 1629–1662.
6. Zapf, A.; Beller, M. The development of efficient catalysts for palladium-catalyzed coupling reactions of aryl halides. *Chem. Commun.* **2005**, 431–440.
7. Christmann, U.; Vilar, R. Monoligated palladium species as catalysts in cross-coupling reactions. *Angew. Chem. Int. Ed.* **2005**, *44*, 366–374.
8. Trzeciak, A.M.; Ziolkowski, J.J. Structural and mechanistic studies of Pd-catalyzed C-C bond formation: The case of carbonylation and Heck reaction. *Coor. Chem. Rev*. **2005**, *249*, 2308–2322.
9. Matsubara, T.; Hirao, K. Density functional study of the σ and π bond activation at the Pd=X (X = Sn, Si, C) bonds of the $(H_2PC_2H_4PH_2)Pd{=}XH_2$ complexes. is the bond cleavage homolytic or heterolytic? *J. Am. Chem. Soc*. **2002**, *124*, 679–689.
10. Albano, V.G.; Bandini, M.; Moorlag, C.; Piccinelli, F.; Pietrangelo, A.; Tommasi, S.; Umani-Ronchi, A.; Wolf, M.O. Electropolymerized Pd-containing thiophene polymer: A reusable supported catalyst for cross-coupling reactions. *Organometallics* **2007**, *26*, 4373–4375.
11. Braga, A.A.C.; Ujaque, G.; Maseras, F. A DFT Study of the full catalytic cycle of the suzuki-miyaura cross-coupling on a model system. *Organometallics* **2006**, *25*, 3647–3658.
12. Sicre, C.; Braga, A.A.C.; Maseras, F.; Cid, M.M. Mechanistic insights into the transmetalation step of a Suzuki-Miyaura reaction of 2(4)-bromopyridines: characterization of an intermediate. *Tetrahedron* **2008**, *64*, 7437–7443.
13. Meir, R.; Kozuch, S.; Uhe, A.; Shaik, S. How can theory predict the selectivity of palladium-catalyzed cross-coupling of pristine aromatic molecules? *Chem. Eur. J*. **2011**, *17*, 7623–7631.
14. Goossen, L.J.; Koley, D.; Hermann, H.L.; Thiel, W. The palladium-catalyzed cross-coupling reaction of carboxylic anhydrides with arylboronic acids: A DFT study. *J. Am. Chem. Soc*. **2005**, *127*, 11102–11114.
15. Goossen, L.J.; Koley, D.; Hermann, H.L.; Thiel, W. Palladium monophosphine intermediates in catalytic cross-coupling reactions: A DFT study. *Organometallics* **2006**, *25*, 54–57.

16. Arooj, M.; Park, K.; Park, J.K. Effects for charge transfer in Pd(II) complexes along various terminal ligands. *Bull. Korean Chem. Soc*. **2010**, *31*, 3815–3817.
17. Ariafard, A.; Lin, Z.; Fairlamb, I.J.S. Effect of the leaving ligand X on transmetalation of organostannanes (vinylSnR_3) with $L_nPd(Ar)(X)$ in stille cross-coupling reactions. A density functional theory study. *Organometallics* **2006**, *25*, 5788–5794.
18. Montoya, V.; Pons, J.; Garcia-Anton, J.; Solans, X.; Font-Bardia, M.; Ros, J. New (η^3-Allyl)palladium complexes with pyridylpyrazole ligands: Synthesis, characterization, and study of the influence of N1 substituents on the apparent allyl rotation. *Organometallics* **2007**, *26*, 3183–3190.
19. Crociani, B.; Antonaroli, S.; Burattini, M.; Benetollo, F.; Scrivanti, A.; Bertoldini, M. Palladium complexes of 8-(di-*tert*-butylphosphinooxy) quinoline. *J. Organomet. Chem*. **2008**, *693*, 3932–3938.
20. Scrivanti, A.; Bertoldini, M.; Beghetto, V.; Matteoli, U.; Venzo, A. Protonation of palladium(II)-allyl and palladium(0)-olefin complexes containing 2-pyridyldiphenylphosphine. *J. Organomet. Chem*. **2009**, *694*, 131–136.
21. Park, S.W.; Chun, Y.; Cho, S.J.; Lee, S.; Kim, K.S. Design of carbene-based organocatalysts for nitrogen fixation: theoretical study. *J. Chem. Theory Comput*. **2012**, *8*, 1983–1988.
22. Faller, J.W.; Wilt, J.C. Palladium/BINAP(S)-catalyzed asymmetric allylic amination. *Org. Lett*. **2005**, *7*, 633–636.
23. Gladiali, S.; Taras, R.; Ceder, R.M.; Rocamora, M.; Muller, G.; Solans, X.; Font-Bardia, M. Asymmetric allylic alkylation catalyzed by Pd(II)-complexes with (*S*)-BINPO, a hemilabile axially chiral P,O-heterodonor inducer. *Tetrahedron Asymmetry* **2004**, *15*, 1477–1485.
24. Chernyshova, E.S.; Goddard, R.; Pörschke, K.-R. Mononuclear NHC-Pd-π-Allyl complexes containing weakly coordinating ligand. *Organometallics* **2007**, *26*, 3236–3251.
25. de Pater, J.J.M.; Tromp, D.S.; Tooke, D.M.; Spek, A.L.; Deelman, B.-J.; van Koten, G.; Elsevier, C.J. Palladium(0)-Alkene Bis(triarylphosphine) complexes as catalyst precursors for the methoxycarbonylation of styrene. *Organometallics* **2005**, *24*, 6411–6419.
26. Canovese, L.; Visentin, F.; Chessa, G.; Uguagliati, P.; Levi, C.; Dolmella, A.; Bandoli, G. Role of the ligand and of the size and flexibility of the palladium-ancillary ligand cycle on the reactivity of substituted alkynes toward Palladium(0) complexes bearing potentially terdentate nitrogen-sulfur-nitrogen or nitrogen-nitrogen-nitrogen ligands: Kinetic and structural study. *Organometallics* **2006**, *25*, 5355–5365.
27. Douthwaite, R.E. Metal-mediated asymmetric alkylation using chiral *N*-heterocyclic carbenes derived from chiral amines. *Coor. Chem. Rev*. **2007**, *251*, 702–717.
28. Sivaramakrishna, A.; Clayton, H.S.; Mogorosi, M.M.; Moss, J.R. Hydrocarbon (π- and σ-) complexesof nickel, palladium and platinum: Synthesis, reactivity and applications. *Coord. Chem. Rev.* **2010**, *254*, 2904–2932.
29. Filipuzzi, S.; Pregosin, P.S.; Albinati, A.; Rizzato, S. Structure, bonding, and dynamics of several palladium η^3-Allyl carbene complexes. *Organometallics* **2008**, *27*, 437–444.
30. Fairlamb, I.J.S.; Kapdi, A.R.; Lee, A.F.; McGlacken, G.P.; Weissburger, F.; de Vries, A.H.M.; Schmieder-van de Vondervoort, L. Exploiting Noninnocent (*E*,*E*)-Dibenzylideneacetone (dba) Effects in Palladium(0)-Mediated cross-coupling reactions: Modulation of the electronic properties of dba affects catalyst activity and stability in ligand and ligand-free reaction systems. *Chem. Eur. J.* **2006**, *12*, 8750–8761.

31. Macé Y.; Kapdi, A.R.; Fairlamb, I.J.S.; Jutand, A. Influence of the dba substitution on the reactivity of Palladium(0) complexes generated from Pd^0_2(dba-*n*,*n*'-Z)$_3$ or Pd^0(dba-*n*,*n*'-Z)$_2$ and PPh_3 in oxidative addition with iodobenzene. *Organometallics* **2006**, *25*, 1795–1800.
32. Köcher, S.; Walfort, B.; Mills, A.M.; Spek, A.L.; Klink, G.P.M.; van Koten, G.; Lang, H. Synthesis and reaction chemistry of 4-nitrile-substituted NCN-pincer palladium(II) and platinum(II) complexes (NCN=[N≡C-4-$C_6H_2(CH_2NMe_2)_2$-2,6]$^-$). *J. Organomet. Chem.* **2008**, *693*, 1991–1996.
33. Blum, K.; Chernyshova, E.S.; Goddard, R.; Jonas, K.; Pörschke, K.-R. 4,9-Diazadodeca-1,trans-6,11-trienes as ligands for Nickel(0), Palladium(0), and Platinum(0). *Organometallics* **2007**, *26*, 5174–5178.
34. Krause, J.; Cestaric, G.; Haack, K.-J.; Seevogel, K.; Storm, W.; Pörschke, K.-R. 1,6-Diene Complexes of Palladium(0) and Platinum(0): Highly reactive sources for the naked metals and [L-M^0] Fragments. *J. Am. Chem. Soc*. **1999**, *121*, 9807–9823.
35. Pla-Quintana, A.; Torrent, A.; Dachs, A.; Roglans, A.; Pleixats, R.; Moreno-Manas, M.; Parella, T.; Benet-Buchholz, J. Chiral and stable Palladium(0) complexes of polyunsaturated Aza-macrocyclic Ligands: Synthesis and Structural analysis. *Organometallics* **2006**, *25*, 5612–5620.
36. Grundl, M.A.; Kennedy-Smith, J.J.; Trauner, D. Rational design of a chiral Palladium(0) olefin complex of unprecedented stability. *Organometallics* **2005**, *24*, 2831–2833.
37. Hunter, G.; McAuley, A.; Whitcombe, T.W. Crystal and Solution Structure of the Palladium(II) Bis(1,4,7-triazacyclononane) Ion: Evidence for rapid fluxional behavior in a macrocyclic complex. *Inorg. Chem*. **1988**, *27*, 2634–2639.
38. Scrivanti, A.; Beghetto, V.; Matteoli, U.; Antonaroli, S.; Marini, A.; Mandoj, F.; Paolesse, R.; Crociani, B. Iminophosphine-palladium(0) complexes as highly active catalysts in the Suzuki reaction. Synthesis of undecaaryl substituted corroles. *Tetrahedron Lett.* **2004**, *45*, 5861–5864.
39. Scrivanti, A.; Beghetto, V.; Matteoli, U.; Antonaroli, S.; Marini, A.; Crociani, B. Catalytic activity of η^2-(olefin)palladium(0) complexes with iminophosphine ligands in the Suzuki-Miyaura reaction. Role of the olefin in the catalyst stabilization. *Tetrahedron* **2005**, *61*, 9752–9758.
40. Arca, M.; Blake, A.J.; Lippolis, V.; Montesu, D.R.; McMaster, J.; Tei, L.; Schroeder, M. Coordination Chemistry of Nitrile and Amino Pendant Arm Derivatives of [9]aneN_2S and [9]aneNS_2 with Pd^{II} and Cu^{II}. *Eur. J. Inorg. Chem.* **2003**, 1232–1241.
41. Albano, V.G.; Bandini, M.; Barbarella, G.; Melucci, M.; Monari, M.; Piccinelli, F.; Tommasi, S.; Umani-Ronchi, A. Controlling stereochemical outcomes of asymmetric processes by catalyst remote molecular functionalizations: Chiral Diamino-Oligothiophenes (DATs) as ligands in asymmetric catalysis. *Chem. Eur. J.* **2006**, *12*, 667–675.
42. Broering, M.; Brandt, C.D. A five coordinate Pd^{II} complex stable in solution and in the solid state. *Chem. Commun*. **2003**, 2156–2157.
43. Park, J.K.; Cho, Y.G.; Lee, S.S.; Kim, B.G. Geometrical characteristics and atomic charge variations of Pd(II) complexes [Pd(L)Cl_2] with an Axial (Pd…O) interaction. *Bull. Korean Chem. Soc*. **2004**, *25*, 85–89.
44. Yoo, J.S.; Ha, D.S.; Kim, J.S.; Kim, B.G.; Park, J.K. Geometrical characteristics and reactivities of tetracoordinated Pd complexes: Mono- and bidentate ligands and charged and uncharged ligands. *Bull. Korean Chem. Soc*. **2008**, *29*, 627–640.

45. Arooj, M.; Park, J.K. Geometrical Structures of the first solvation shell of the $[PdCl_4]^{2-}$ core: charge-dipole *vs.* dipole-dipole interaction of (Pd^{II}...Solvent). *Bull. Korean Chem. Soc*. **2008**, *29*, 2295–2298.
46. Ayala, R.; Marcos, E.S.; Dĭaz-Moreno, S.; Solė, V.A.; Muñoz-Păez, A. Geometry and hydration structure of Pt(II) square planar complexes $[Pt(H_2O)_4]^{2+}$ and $[PtCl_4]^{2-}$ as studied by X-ray absorption spectroscopies and quantum-mechanical computations. *J. Phys. Chem. B* **2001**, *105*, 7588–7593.
47. Burda, J.V.; Zeizinger, M.; Leszczynski, J. Activation barriers and rate constants for hydration of platinum and palladium square-planar complexes: An *ab initio* study. *J. Chem. Phys.* **2004**, *120*, 1253–1262.
48. Frish, M.J.; Trucks, G.W.; Head-Gordon, M.H.; Gill, P.M.W.; Wong, M.W.; Foresman, J.B.; Johnson, B.G.; Schlegel, H.B.; Robb, M.A.; Replogle, E.S.; *et al*. *Gaussian 03*; Gaussian Inc.: Pittsburgh, PA, USA, 2003.
49. Becke, A.D. *The Challenge of d- and f-Electrons: Theory and Computation*; ACS Symposium Series, No. 394; Salahub, D.R., Zerner, M.C., Eds.; American Chemical Society: Washington, DC, USA, 1989; p. 166.
50. Becke, A.D. Density-functional exchange-energy approximation with correct asymptotic behavior. *Phys. Rev.* **1988**, *A38*, 3098–3100.
51. Perdew, J.P. Transport and relaxation of hot conduction electrons in an organic dielectric. *Phys. Rev.* **1986**, *B33*, 8822–8824.
52. Search Chemistry WebElements, WebElements Periodic Table of the Elements (the periodic table on the web). Available online: http://www.webelements.com (accessed on 10 July 2011).
53. Blake, A.J.; Holder, A.J.; Hyde, T.I.; Roberts, Y.V.; Lavery, A.J.; Schroeder, M. Structural and electrochemical studies on trithia macrocyclic complexes of palladium. *J. Organomet. Chem*. **1987**, *323*, 261–270.
54. Lai, Y.-H.; Ma, L.; Mok, K.F. Synthesis and conformational and complexation studies of 2,17-dioxa-5,14-dithia[6.6] orthocyclophane. A ligand with monodentate and bidentate properties. *New J. Chem*. **1997**, *21*, 985–991.
55. Pinkas, J.; Huffman, J.C.; Chisholm, M.H.; Caulton, K.G. Origin of different coordination polyhedra for $Cu[CF_3C(O)CHC(O)CF_3]_2L$ ($L = H_2O$, NH_3). *Inorg. Chem.* **1995**, *34*, 5314–5318.
56. Kozelka, J.; Bergès, J.; Attias, R.; Fraitag, J. O-H…Pt^{II}: Hydrogen bond with a strong dispersion component. *Angew. Chem. Int. Ed*. **2000**, *39*, 198–201.
57. Miessler, G.L.; Tarr, D.A. *Inorganic Chemistry*, 3rd ed.; Pearson Prentice Hall, Pearson Education, Inc.: Upper Saddle River, NJ, USA, 2004; pp. 337–376.
58. Albight, T.A.; Burdett, J.K.; Whangbo, M.-Y. *Orbital Interactions in Chemistry*; Wiley-Interscience: New York, NY, USA, 1985; pp. 295–296.

Sample Availability: Samples of the compounds are available from the authors.